Metamorphic CO2 production in calc-silicate rocks from the eastern Himalaya

Journal:	*Italian Journal of Geosciences*
Manuscript ID	IJG-2015-0423.R2
Manuscript Type:	Original Article
Date Submitted by the Author:	n/a
Complete List of Authors:	Rolfo, Franco; University of Torino, Department of Earth Sciences Groppo, Chiara; University of Torino, Department of Earth Sciences Mosca, Pietro; CNR, IGG
Keywords:	Metamorphic CO2, Himalaya, Metacarbonate rocks

SCHOLARONE™
Manuscripts

1
2
3
4
5
6
7
8
9
10
11
12
13
14
15
16
17
18
19
20
21
22
23
24
25
26
27
28
29
30
31
32
33
34
35
36
37
38
39
40
41
42
43
44
45
46
47
48
49
50
51
52
53
54
55
56
57
58
59
60

Metamorphic CO_2 production in calc-silicate rocks from the eastern Himalaya

Franco Rolfo[1,2], Chiara Groppo[1,2], Pietro Mosca[2]

1 Department of Earth Sciences, University of Torino, Italy

2 IGG - CNR, Torino, Italy

Abstract

Metamorphic degassing from active collisional orogens may supply a significant fraction of the global solid-Earth derived CO_2 to the atmosphere, thus playing a fundamental role even in today's Earth carbon cycle. The Himalayan belt, a major active collisional orogen, is a good candidate for the production of large amounts of metamorphic CO_2 that may influence the long-term climate. Metamorphic CO_2 can be produced during prograde metamorphism of impure carbonate rocks. However, reliable quantitative modeling of metamorphic CO_2 fluxes from the Himalayan belt requires a good knowledge of the nature, magnitude and distribution of the CO_2-producing processes.

This study focuses on the metamorphic decarbonation processes occurring during the Himalayan collision, with special focus on the distribution of different types of metacarbonate rocks in the Eastern Himalaya and their petrographic description. Petrological data about selected CO_2-producing reactions suggest that the most common calc-silicate rocks are potential great sources of metamorphic CO_2, the molar amount of CO_2 in the fluid ranging between 37 and 44 % in CFMAS-HC lithologies and between 21 and 57 % in NKCFMAS-HC lithologies. These results contribute to a better understanding of the influence exerted by orogenic processes on climatic changes at global scale.

Keywords: Orogenic CO_2; Climate changes; Decarbonation processes; Himalaya; Metacarbonate rocks.

Introduction and aim of the study

Metamorphic degassing from active collisional orogens is suspected to supply significant amounts of CO_2 to the atmosphere, thus playing a fundamental role in the long-term (>1 Ma) global carbon cycle (e.g. KERRICK & CALDEIRA, 1993; SELVERSTONE & GUTZLER, 1993; BICKLE, 1996; BERNER, 1999; MÖRNER & ETIOPE, 2002; GAILLARDET & GALY, 2008; EVANS, 2011).

A number of parameters could positively influence the extent of metamorphic degassing; among them, of major importance are the occurrence of appropriate lithologies, the size of the orogens and the maximum temperatures reached during their metamorphic evolution. The Himalaya is the largest "large-hot" collisional orogen on Earth (BEAUMONT *et alii*, 2010), over 2500 km wide along strike and rich in high grade metamorphic rocks. Moreover, tectonic and erosional processes are still active today. Therefore, the Himalaya is a likely candidate for the production of a huge amount of metamorphic CO_2 that may have contributed to changes in long-term climate of the past and that may still influence the atmospheric composition in the near future (e.g. GAILLARDET & GALY, 2008; GIRAULT *et alii*, 2014).

In a somehow over-simplified conceptual scheme, large metamorphic CO_2 fluxes should have been (and should still be) facilitated by rapid metamorphism of large volumes of metacarbonate rocks, coupled with facile escape of CO_2 to the Earth's surface. However, the nature, magnitude and distribution of the CO_2-producing processes in Himalaya, is still poorly known. It is therefore difficult to build a reliable quantitative modeling of metamorphic CO_2 fluxes in the Himalaya, as well as in any other collisional orogen (e.g. MÖRNER & ETIOPE, 2002).

The key to understanding the metamorphic CO_2 flux in the past, is to investigate the petrologic evolution of the calc-silicate CO_2-source rocks currently exposed on the Earth surface. Within the framework of several projects, our research group focused on the metamorphic decarbonation processes occurring during the evolution of the Himalayan orogen (ROLFO *et alii*, 2015). Fieldwork activity was combined with petrographic, petrologic, structural, geochronological, geochemical and fluid inclusion studies with the aims of clarifying: (i) abundance and types of CO_2-source rocks, (ii)

nature and rate of CO_2-producing reactions, (iii) nature, composition and amounts of the released CO_2-rich fluids, (iv) nature and distribution of the CO_2 escape-paths toward the Earth's surface, and (v) chronology of metamorphic CO_2-producing reactions occurred in the Himalayas at different structural levels and at different times.

In this paper we present our results on points (i) to (iii): the distribution and petrography of the different types of metacarbonate rocks in the Eastern Himalaya is reported in detail for the first time, and petrological evidence on the nature of the CO_2-producing reactions in different types of calc-silicate rocks is summarized and discussed in the global perspective of the orogenic CO_2-cycle.

Field descriptions of metacarbonate rocks in eastern Himalaya

A number of authors recognized calc-silicate rocks among the most common lithologies in the Greater Himalayan Sequence (GHS), which is the core of the Himalayan metamorphic belt and consists of medium- to high-grade micaschist and paragneiss and of granitic orthogneiss showing pervasive evidence of anatexis (e.g. LOMBARDO *et alii*, 1993; CAROSI *et alii*, 1999; SEARLE *et alii*, 2003; GOSCOMBE *et alii* 2006; LONG *et alii*, 2011; MOSCA *et alii*, 2011, 2014; ROLFO *et alii*, in press). However, these lithologies have been understudied so far, mainly because they are notoriously difficult to be studied by means of petrologic modeling.

In the eastern Himalaya, calc-silicate rocks are widespread in the lower and upper structural levels of the GHS (MOSCA *et alii*, 2013). In selected localities, calc-silicate rocks outcrop even at mountain scale, with notable examples occurring for instance in the Everest and Makalu national parks (Fig. 1).

At the outcrop scale, calc-silicate rocks are easy to map and usually show very characteristic deformation styles because of their relatively weak rheological behavior compared to the host quartz-feldspar rich rocks. In hand specimen, calc-silicate rocks vary in appearance according to their modal composition and relative abundance of various Ca-rich minerals (Fig. 2). They are often banded at a centimetre to decimetre scale and the most typical textures include granoblastic

structures. The most abundant minerals are anorthite-rich plagioclase and diopsidic pyroxene. Assemblages also include additional Ca-Mg-Fe-rich silicates (e.g. Ca-amphibole, grossular-rich garnet, zoisite), Na-Ca solid solutions (e.g. scapolite) and locally abundant K-rich minerals (e.g. white mica, biotite, K-feldspar). Garnet- and clinopyroxene- rich / plagioclase-poor varieties of calc-silicate rocks with abundant clinopyroxene+plagioclase intergrowths are quite similar to the retrogressed eclogites described in eastern Himalaya (LOMBARDO & ROLFO, 2000). However, these calc-silicate rocks may be clearly recognized on the basis of minerals composition (always Ca-rich), occurrence of scapolite and relative abundance of titanite, and should thus not be confused with eclogites (see for instance the samples described by CORRIE *et alii*, 2010).

Field data acquired in over 10 years in central-eastern Nepal and Sikkim allowed us to distinguish two main different modes of occurrence at the different structural levels in the GHS (Fig. 3), as preliminary outlined by Rolfo *et alii* (2015):

(i) in the lower portion of the GHS (GHS-L), calc-silicate rocks generally occur as decimetre to metre-thick layers or massive boudins (Fig. 4a,b,c) enveloped by the main foliation of the hosting medium- to high-grade, locally anatectic, staurolite- and/or kyanite-bearing metapelites (e.g. GROPPO *et alii*, 2009; MOSCA *et alii*, 2012);

(ii) in the structurally higher portion of the GHS (GHS-U), calc-silicate rocks are hosted in anatectic kyanite-sillimanite- bearing gneisses (i.e. Barun Gneiss, see GROPPO *et alii* 2012) and often occur as tens to hundreds of metres thick, folded or boudinated, levels occasionally associated with layers of impure marbles (Fig. 4a,d,e).

Where preserved, the original transition between the host paragneiss and the calc-silicate granofels is generally gradual and is characterized by the progressive disappearance of biotite and the appearance of calc-silicate minerals. A banded structure is often observed in the calc-silicate rocks, which is defined by the different modal proportion of the rock-forming minerals in adjacent layers. These features suggest that the calc-silicate rocks derive from former marly intercalations within a thick sedimentary sequence.

The calc-silicate rocks are characterized by different mineral assemblages that vary systematically as a function of the structural level and of the protolith composition (Fig. 3); they are described in detail in the next section.

Petrography of different varieties of metacarbonate rocks

The studied samples are medium- to fine-grained and generally have granofelsic structure. An exception includes phyllosilicate-rich schists, and gneisses that have evidence of brittle-to-ductile deformation resulting in local grain size reduction. Two different calc-silicate groups have been recognized, corresponding to different protolith compositions: they can be described in the (1) CFMAS-HC (CaO-FeO-MgO-Al_2O_3-SiO_2-H_2O-CO_2) and (2) NKCFMAS-HC (Na_2O-K_2O-CaO-FeO-MgO-Al_2O_3-SiO_2-H_2O-CO_2) model systems, respectively. The CFMAS-HC calc-silicate rocks are significantly more abundant in the GHS-L than in the GHS-U (Fig. 3); the NKCFMAS-HC calc-silicate rocks are widespread in both the GHS-L and GHS-U, but they occur as thin levels (decimetre- to metre- thick) in the GHS-L whereas they form very thick layers in the GHS-U (up to hundreds of metres thick) (Fig. 4d,e). In both calc-silicate groups, mineral assemblages vary with increasing metamorphic grade from lower to upper structural levels of the GHS.

1. CFMAS-HC assemblages

The following mineral assemblages can be observed from lower to upper structural levels (and from lower to higher metamorphic grade; Table 1):

(A) Tremolite-bearing (clinopyroxene and garnet -absent) impure marbles

These rocks occur as metre-thick layers within two-mica garnet ± staurolite ± kyanite -bearing schists of the GHS-L and have been recognized only sporadically (Fig. 3); their structure vary from granoblastic to slightly foliated. Beside calcite, these marbles are characterized by the presence of tremolite, often occurring as centimetre-long, slightly oriented, poikiloblasts (Fig. 5a) locally replaced by aggregates of talc, and minor graphite.

(B) Garnet + amphibole ± zoisite -bearing (clinopyroxene -absent) calc-silicate rocks

These rocks represent thin layers (centimetre- to decimetre- thick) intercalated with two-mica garnet-bearing schists and gneisses and minor quartzites of the GHS-L. They are characterized by abundant garnet (generally already evident at the outcrop scale), quartz and by the systematic lack of calcite and clinopyroxene. Ca-rich plagioclase, zoisite, green amphibole and accessory titanite are also part of the mineral assemblage (Fig. 5b). Zoisite is locally abundant (up to 30-40 vol%) and is replaced by coarse-grained plagioclase (Fig. 5c).

(C) Garnet + clinopyroxene ± zoisite -bearing calc-silicate rocks

This assemblage is the most abundant in the CFMAS-HC calc-silicate group. These very common rocks occur as thin layers (decimetre-thick) and/or boudins within garnet + K-feldspar + biotite + kyanite ± sillimanite anatectic paragneisses and are widespread in the upper structural levels of the GHS-L. Commonly banded, these rocks display centimetre-thick alternated layers of different mineral modes, compositions and microstructures. These comprise (a) Grt-rich, Cpx-poor (Fig. 5d,e), (b) Cpx-rich, Grt-poor layers. However, the equilibrium assemblage in both layer types consists of plagioclase + clinopyroxene + quartz + garnet ± zoisite; calcite is absent. Titanite and apatite are ubiquitous as accessory minerals. In layer (a), garnet is grossular-rich (Grs_{67-74}) and mainly occurs as large porphyroblasts with a spongy appearance, intimately intergrown with quartz (Fig. 5d,e) and locally partially replacing clinopyroxene rims. Plagioclase is an almost pure anorthite (An_{95-96}). Graphite is abundant and occurs as large flakes concentrated in the plagioclase-rich domains (Fig. 5d,e). Relict zoisite is included in both garnet and clinopyroxene. In layers (b), garnet occurs as: (1) large zoned porphyroblasts with almandine-rich cores and grossular-rich rims (Grs_{71-73}); (2) small blebs and/or idioblasts (Grs_{67-76}) associated with plagioclase. Clinopyroxene forms large, weakly zoned crystals, locally intergrown with plagioclase.

In summary, microstructural evidence suggest that garnet grew at the expense of zoisite, clinopyroxene and calcite, the latter being only locally observed as inclusion in garnet. Notably, coarse-grained graphite has been interpreted as precipitated from a H_2O-CO_2 fluid released through

decarbonation reactions during prograde and/or early retrograde metamorphic evolution (GROPPO *et alii*, 2013).

(D) Clinopyroxene -bearing (garnet -absent) calc-silicate rocks

These rocks are locally observed as decimetre- to metre-thick layers within garnet + K-feldspar + biotite + sillimanite ± kyanite anatectic paragneisses of the GHS-U, locally associated with type (F) of the NKCFMAS-HC group. They are characterized by a very simple mineral assemblage consisting of quartz, plagioclase and clinopyroxene (Fig. 5f,g), ± very minor calcite, and by the systematic lack of garnet.

2. NKCFMAS-HC assemblages

The following mineral assemblages can be observed from lower to upper structural levels (and from lower to higher metamorphic grade) (Table 1):

(A) Muscovite and/or phlogopite –bearing impure marbles

These rocks crop out as thin (decimetre- to metre thick) layers intercalated with GHS-L two-mica garnet ± kyanite schists, and locally with type (B) lithologies of the NKCFMAS-HC group and type (A) of the CFMAS-HC group. The schistose texture is defined by alignment of muscovite and/or phlogopite (Fig. 6a,b). Quartz, minor plagioclase, rare tremolite and graphite also occur in the main mineral assemblage. Titanite and tourmaline are present as accessory minerals.

(B) Muscovite and/or biotite + calcite -bearing phylladic micaschists

Although not very abundant, this lithology is quite representative and is probably the most common product of medium-grade metamorphism of the former marly protolith. It occurs as thin (decimetre- to metre- thick) layers within two-mica garnet -bearing schists, at the lowermost structural levels of the GHS-L, immediately above the LHS two-mica augen-gneiss (Ulleri orthogneiss). These rocks are characterized by a mixed silicatic and carbonatic assemblage, mainly consisting of quartz, plagioclase, muscovite, biotite and calcite in different modal amounts (Table 1, Fig. 6c,d). Relict porphyroclastic ankerite is locally observed, partially replaced by calcite. Biotite often shows a

greenish-brownish pleochroism (Fig. 6c). Calcite is widespread in the matrix, where it is locally concentrated in millimetre-thick discontinuous domains alternating to the silicate-rich portions (Fig. 6d). Rare phlogopite + actinolite + calcite -rich calc-silicate granofels are associated with these phylladic micaschists and probably represent the metamorphic products of Mg-Fe rich marly intercalations.

(C) Muscovite and/or biotite + zoisite + scapolite + garnet -bearing micaschists

These rocks have been only rarely observed, most probably because at the outcrop scale they resemble normal two-mica + garnet -bearing schists and they can be identified as calc-silicate rocks only under the microscope. They occur as thin (centimetre- to decimetre- thick) layers associated with (or at the same structural level than) type (B) of the NKCFMAS-HC group. The most common feature of these rocks is the presence of abundant Ca-rich plagioclase, zoisite and/or scapolite (i.e. calc-silicate minerals) in addition to the two-mica + garnet assemblage commonly found in the metapelites at these structural levels (Fig. 6e,f). Microstructural relationships suggest that zoisite is replaced by Ca-rich plagioclase, which is in turn replaced by scapolite. Calcite is absent, probably because it has been completely consumed during metamorphism. Titanite is a common accessory mineral.

(D) Biotite and/or K-feldspar + scapolite -bearing calc-silicate gneisses

Similarly to the previous type (C), these rocks are not easy to be identified in the field. Macroscopically, they resemble the common biotite + garnet -bearing gneisses to whom they are associated; calc-silicate minerals can be identified only under the microscope. They occur as metre-thick layers within the biotite + K-feldspar + garnet + kyanite ± sillimanite gneisses, locally anatectic, cropping out at the uppermost structural levels of the GHS-L, and are often associated with the type (E) of the NKCFMAS-HC calc-silicate group. These rocks generally show a gneissic texture due to abundance of biotite which is mostly concentrated in discontinuous layers; a typical character is the presence of scapolite in an otherwise common mineral assemblage consisting of

quartz, plagioclase, biotite, ± K-feldspar, ± clinozoisite/epidote (Fig. 6g,h). Titanite is ubiquitous; calcite is absent.

(E) Biotite and/or K-feldspar + scapolite + clinozoisite + amphibole + clinopyroxene -bearing calc-silicate gneisses

Often associated with the type (D) of the NKCFMAS-HC calc-silicate group, these calc-silicate gneisses are quite easy to be recognized in the field due to the presence of abundant green amphibole and minor clinopyroxene. The presence of this amphibole in the equilibrium assemblage is the most common feature of this calc-silicate type (Fig. 6i,j). The abundant biotite is in some places replaced by K-feldspar (Fig. 6i). The calc-silicate assemblage includes plagioclase, clinozoisite and minor scapolite (Fig. 6i,j). Clinopyroxene is less abundant than amphibole. Titanite is the most common accessory mineral.

(F) K-feldspar + scapolite + clinopyroxene ± zoisite ± calcite -bearing calc-silicate rocks

This assemblage is the most abundant among the NKCFMAS-HC calc-silicate group. These very common rocks occur as thick (tens to hundreds of metres-thick) layers within the GHS-U garnet + biotite + K-feldspar + sillimanite ± kyanite anatectic gneisses (Barun gneisses); calcite-rich layers (impure marbles) are locally intercalated with predominant calcite-poor layers (calc-silicate rocks). The main mineral assemblage consists of K-feldspar + clinopyroxene + scapolite ± zoisite ± calcite ± minor quartz (Fig. 6k,l). Relict biotite often occurs within clinopyroxene and/or is replaced by K-feldspar. Clinopyroxene (Di_{67-72}) is often partially replaced by retrograde green Ca-amphibole ± epidote ± calcite (Fig. 6k), whereas scapolite ($eqAn_{66-69}$) is locally partially to completely replaced by aggregates of plagioclase + calcite and/or it is overgrown by coarse-grained epidote (Fig. 6k,l). In addition to the ubiquitous titanite, a strongly pleochroic allanite and a bluish to colorless tourmaline locally occur, whereas graphite is always absent.

Metamorphic evolution and CO_2-producing processes in calc-silicate rocks

The nature of the CO_2-producing reactions in the most abundant types of each calc-silicate group (i.e. type (C) representative of the CFMAS-HC group and type (F) for the NKCFMAS-HC group) has been petrologically investigated in the appropriate model systems using isobaric T-X(CO_2) phase diagram sections and/or pseudosections, and phase diagram projections in which fluid composition is not explicitly constrained (for a full description of methods and results, see GROPPO *et alii*, 2013; GROPPO *et alii*, submitted). Independently from the model system, the relevant CO_2-producing reactions are either "truly" univariant reactions (i.e. effectively univariant in the P-T space and corresponding to isobaric invariant points in the T-X(CO_2) space) or isobaric univariant reactions (i.e. divariant in the P-T space). In the following, the main results of these petrologic studies are summarized.

CFMAS-HC group: type C (Grt + Cpx ± Zo –bearing) calc-silicate rocks

The P-T evolution of the studied samples was derived from that of the hosting GHS-L anatectic paragneiss (GROPPO *et alii*, 2009), which experienced peak P–T conditions of 780–800°C and 10.5–11.0 kbar, followed by decompression to ca. 8.5–9.0 kbar associated with moderate cooling to ca. 750°C.

The petrological results, described in detail by GROPPO *et alii* (2013), define the P-T-X^{fluid} regime during the metamorphic evolution of the studied calc-silicate rocks (Fig. 7a,c). The relevant CO_2-producing reactions occurred during prograde heating up to peak-T of about 800°C (at about 10-11 kbar) and/or early decompression. These reactions involved the growth of grossular-rich garnet (Grs_{67-81}) in equilibrium with quartz at the expenses of zoisite, clinopyroxene and calcite (*isobaric univariant reaction 24b* in Fig. 7a), and in equilibrium with plagioclase and quartz at the expenses of zoisite, clinopyroxene and calcite (*"truly" univariant reaction U26c* in Fig. 7c). The modelled reactions are fully consistent with the observed microstructures and measured mineral compositions. Both these reactions released a CO_2-rich fluid (XCO_2=0.32-0.44 and XCO_2=0.37-0.48, respectively; Fig. 7a,c).

The systematic occurrence of large and abundant graphite flakes suggests that graphite may have precipitated from the CO_2-rich C–O–H fluid internally produced through the garnet-forming reactions. Two possible graphite precipitation mechanisms may be envisaged: (i) T decrease and/or P increase; (ii) X^{fluid} variation to enter the graphite stability field. Hydration reactions at constant P and T would represent a mechanism capable of changing the composition of the fluid in an internally buffered system; the widespread occurrence of hydrated minerals associated with graphite support the possibility that precipitation of graphite was triggered by hydration reactions. Moreover, GROPPO *et alii* (2013) demonstrated that the observed graphite modes (ca. 1 vol%) are comparable with those directly related to the estimated amount of decarbonation, strongly suggesting that the studied calc-silicate rocks behaved as a closed system during their prograde and early retrograde evolution.

NKCFMAS-HC group: type F (Kfs + Scp + Cpx ± Zo ± Cal –bearing) calc-silicate rocks

The GHS-U scapolite-bearing calc silicates experienced isobaric heating at ca. 9 kbar to peak temperature conditions of 780-800°C followed by nearly isothermal decompression to ca. 7 kbar (Fig. 7d), as defined by the hosting anatectic paragneiss (Barun Gneiss: GROPPO *et alii*, 2012).

Thermodynamic modeling (Groppo *et alii*, submitted) demonstrates that the observed microstructures in this rock type reflect either isobaric univariant assemblages or isobaric invariant assemblages. The CO_2-rich fluid was released through several prograde reactions, depending on the local bulk composition, involving the growth of clinopyroxene, K-feldspar, and zoisite and the consumption of scapolite (eqAn=0.64-0.67), quartz and calcite. The modeled reactions are fully consistent with the observed microstructures and measured mineral compositions. These CO_2-producing reactions are "truly" univariant reactions (i.e. they correspond to isobaric invariant points in the isobaric T-XCO_2 sections) (Fig. 7b, d).

The first univariant curve crossed during the prograde evolution is the *clinopyroxene-forming reaction U20a* in Fig. 7d (Cal + Pl + Qtz + Tr + Zo = Di + Scp + F). This reaction was crossed at

about 590°C and released a fluid relatively rich in CO_2 (XCO_2 = 0.21-0.28). At higher T (ca. 650°C), both the *zoisite- and K-feldspar-producing reaction U10d* (Qtz + Cal + Mu + Scp = Zo + Pl + Kfs + F) (Fig. 7d) and the *clinopyroxene- and K-feldspar-producing reaction U33c* (Cal + Phl + Qtz + Scp + Zo = Di + Kfs + Pl + F) (Fig. 7d) were crossed at ca. 650°C (Fig. 7d), both releasing a CO_2-rich fluid (XCO_2 = 0.51-0.57).

These preliminary results demonstrate that: (i) Kfs + Scp + Cpx ± Zo ± Cal -bearing calc-silicate rocks may act as a CO_2-source during prograde heating, releasing internal-derived CO_2-rich fluids; (ii) the role of phases such as zoisite, scapolite and plagioclase solid solutions must be taken in account whenever a quantitative and reliable estimate of the CO_2-producing metamorphic processes in orogenic zones is sought.

Discussion and conclusions

In the eastern Himalaya, calc-silicate rocks are widespread in the lower and upper structural levels of the GHS. Gathering of field data, coupled with new petrographic observations indicate that two main groups of calc-silicate assemblages reflect differences in the protolith composition: CFMAS-HC assemblages, more abundant in the GHS-L, and NKCFMAS-HC assemblages, volumetrically more significant in the GHS-U. Many of these assemblages, especially those equilibrated at lower temperatures and still containing abundant phyllosilicates, are not easy to recognize in the field and probably have been considerably overlooked in the past. These assemblages do not usually contain calcite, because calcite was completely consumed during prograde metamorphism; nevertheless, it is proved that they played an important role in the orogenic-CO_2 cycle.

The petrologic studies summarized in this paper demonstrate that both CFMAS-HC and NKCFMAS-HC calc-silicate groups act as a significant CO_2-source during prograde heating and/or early decompression near peak conditions, releasing internal-derived CO_2-rich fluids through garnet-forming (CFMAS-HC) and clinopyroxene + K-feldspar -forming and scapolite -consuming

(NKCFMAS-HC) reactions. The molar amount of CO_2 in the fluid ranges between 37 and 44 % in CFMAS-HC lithologies and between 21 and 57 % in NKCFMAS-HC lithologies.

A potentially very important result of our petrologic modeling is that, if the system remains closed, fluid-rock interactions may induce hydration of the calc-silicate assemblages (mainly plagioclase and clinopyroxene) and in-situ graphite precipitation, thereby removing carbon from the fluid. This seem to be the case for the graphite-bearing CFMAS-HC calc-silicate rocks in the GHS-L, which likely behaved as a closed-system during their prograde and early retrograde evolution, although their volume abundance within the hosting paragneiss is relatively low.

The interplay between these two contrasting processes – i.e. production of metamorphic CO_2-rich fluids vs. carbon sequestration through graphite precipitation – must be taken in account when dealing with a global estimate of the role exerted by decarbonation processes on the orogenic CO_2-cycle.

Extending these results in the global perspective of the orogenic CO_2-cycle will require additional studies to quantitatively define the volumetric amount of the different varieties of CO_2-source rocks within the GHS throughout the Himalayan orogen, as well as within other orogens. Moreover, precise geochronology on the peak assemblages resulting from the CO_2-producing reactions in the different types of calc-silicate rocks will help to constrain the possible occurrence of CO_2 major influxes in the past.

References

BEAUMONT C., JAMIESON R. & NGUYEN M. (2010) - *Models of large, hot orogens containing a collage of reworked and accreted terranes,* Canadian Journal of Earth Sciences, **47,** 485-515.

BERNER R.A. (1999) - *A new look at the long-term carbon cycle,* GSA Today, **9/11,** 1–6.

Bickle M.J. (1996) - *Metamorphic decarbonation, silicate weathering and the long-term carbon cycle,* Terra Nova, **8,** 270–276.

CAROSI R., LOMBARDO B., MUSUMECI G. & PERTUSATI P.C. (1999) - *Geology of the Higher Himalayan Crystallines in Khumbu Himal (Eastern Nepal),* Journal of Asian Earth Sciences, **17,** 785-803.

CORRIE S.L., KOHN M.J. & VERVOORT J.D. (2010) - *Young eclogite from the Greater Himalayan Sequence, Arun Valley, eastern Nepal: P–T–t path and tectonic implications,* Earth and Planetary Science Letters, **289,** 406–416.

DASGUPTA S., GANGULY J. & NEOGI S. (2004) - *Inverted metamorphic sequence in the Sikkim Himalayas: crystallization history, P–T gradient and implications,* J. metamorphic Geol., **22,** 395–412.

EVANS K.A. (2011) - *Metamorphic carbon fluxes: how much and how fast?* Geology, **39,** 95–96.

GAILLARDET J. & GALY A. (2008) – *Himalaya -- carbon sink or source?* Science, **320,** 1727–1728.

GIRAULT F., PERRIER F., CROCKETT R., BHATTARAI M., KOIRALA B.P., FRANCE-LANORD C., AGRINIER P., ADER M., FLUTEAU F., GRÉAU C. & MOREIRA M. (2014) - *The Syabru-Bensi hydrothermal system in central Nepal: 1. Characterization of carbon dioxide and radon fluxes,* Journal of Geophysical Research, Solid Earth, **119,** 4017-4055.

GOSCOMBE B., GRAY D. & HAND M. (2006) - *Crustal architecture of the Himalayan metamorphic front in eastern Nepal,* Gondwana Res., **10,** 232–255.

GROPPO C., ROLFO F. & LOMBARDO B. (2009) - *P-T evolution across the Main Central Thrust Zone (East-ern Nepal): hidden discontinuities revealed by petrology,* J. Petrol., **50,** 1149–1180.

GROPPO C., ROLFO F. & INDARES A. (2012) - *Partial melting in the Higher Himalayan Crystallines of Eastern Nepal: the effect of decompression and implications for the ''channel flow'' model,* J. Petrol., **53,** 1057–1088.

GROPPO C., ROLFO F., CASTELLI D. & CONNOLLY J.A.D. (2013) - *Metamorphic CO_2 production from calc-silicate rocks via garnet-forming reactions in the CFAS-H_2O-CO_2 system,* Contrib. Mineral. Petrol., **166,** 1655–1675.

GROPPO C., ROLFO F., MOSCA P. & CASTELLI D. (submitted) - *Metamorphic CO_2 production in collisional orogens: petrologic constraints from Cpx+Kfs+Scp+Zo-bearing calc-silicate rocks investigated in the NKCMAS-HC system.* Contrib. Mineral. Petrol.

KERRICK D.M. & CALDEIRA K. (1993) - *Paleoatmospheric consequences of CO_2 released during early Cenozoic regional metamorphism in the Tethyan orogen,* Chem. Geol., **108,** 201–230.

LOMBARDO B., PERTUSATI P. & BORGHI A. (1993) - *Geology and tectono-magmatic evolution of the eastern Himalaya along the Chomolungma-Makalu transect,* In: TRELOAR, P. J. & SEARLE M.P. (eds.) - *Himalayan Tectonics,* Geological Society of London, Special Publication, **74,** 341–355.

LOMBARDO B. & ROLFO F. (2000) - *Two contrasting eclogite types in the Himalayas: implications for the Himalayan orogeny,* Journal of Geodynamics, **30,** 37-60.

LONG S., MCQUARRIE N., TOBGAY T., GRUJIC D. & HOLLISTER L. (2011) - *Geologic Map of Bhutan,* Journal of Maps, **7,** 184-192.

MÖRNER N.A. & ETIOPE G. (2002) - *Carbon degassing from the lithosphere,* Global and Planetary Change, **33,** 185-203.

MOSCA P., GROPPO C. & ROLFO F. (2011) - *Geological and structural architecture of the Kangchenjunga region in Eastern Nepal,* Journal of Nepal Geological Society, **43,** 1-12.

MOSCA P., GROPPO C. & ROLFO F. (2012) - *Structural and metamorphic features of the Main Central Thrust Zone and its contiguous domains in the eastern Nepalese Himalaya,* Journal of the Virtual Explorer, **41,** paper 2.

MOSCA P., GROPPO C. & ROLFO F. (2013) - *Main geological features of the Rolwaling-Khumbu Himal between the Khimti Khola and Dudh Khosi valleys (eastern-central Nepal Himalaya),* Rend. Online Soc. Geol. It., **29,** 112-115.

MOSCA P., GROPPO C. & ROLFO F. (2014) - *The geology between Khimti Khola and Likhu Khola valleys: a field trip along the Numbur Cheese Circuit (central-eastern Nepal Himalaya),* In: C. MONTOMOLI, R. CAROSI, R. LAW, S. SINGH, S.M. RAI (eds.), *Geological field trips in the Himalaya, Karakoram and Tibet,* Journal of the Virtual Explorer, **47,** paper 4.

ROLFO F., GROPPO C., MOSCA P., FERRANDO S., COSTA E. & KAPHLE K.P. (2015) - *Metamorphic CO_2 degassing in the active Himalayan orogen: exploring the influence of orogenic activity on the long-term global climate changes,* In: G. LOLLINO et al. (eds.), *Engineering Geology for Society and Territory,* Volume 1, 21-25. Springer International Publishing Switzerland.

ROLFO F., GROPPO C. & MOSCA P. (in press) - *Petrological constraints of the "Channel Flow" model in eastern Nepal,* In: MUKHERJEE, S., CAROSI, R., VAN DER BEEK, P. A., MUKHERJEE, B. K. & ROBINSON, D. M. (eds) *Tectonics of the Himalaya*, Geological Society, London, Special Publications, **412**. http://dx.doi.org/10.1144/SP412.4

SEARLE M.P., SIMPSON R.L., LAW R.D., PARRISH R.R. & WATERS D.J. (2003) - *The structural geometry, metamorphic and magmatic evolution of the Everest massif, High Himalaya of Nepal–South Tibet,* Journal of the Geological Society, London, **160,** 345-366.

SELVERSTONE J. & GUTZLER D.S. (1993) - *Post- 125 Ma carbon storage associated with continent-continent collision,* Geology, **21,** 885–888.

FIGURES CAPTIONS

Fig. 1 - Well know occurrences of calc-silicate rocks at large scale in eastern Himalaya: **(a)** the world-famous ridge between Nupse and Lhotse in upper Khumbu Himal shows very clear yellowish bands (arrow) embedded and deformed within dark rocks of the Everest Series; **(b)** the same bands are clearer when seen from the east, from the upper Barun Valley at the Makalu Base camp; **(c)** in the lower Barun Valley of East Nepal, the lower portion of the left valley side is carved among calc-silicate rocks, gently dipping to the left (west) along a distance of several kilometres ; **(d)** in central Sikkim, Pandim (6691 m) west face reveals huge volumes of calc silicate rocks embedded within whitish leucogranites and other dark lithologies of the GHS.

Fig. 2 - Calc-silicate rocks structures, according to their modal composition and the relative abundance of various Ca-rich minerals. **(a)** Banded calc-silicate rock, Samiti Lake, Sikkim, NE India. **(b)** Centimetre-thick bands with white granoblastic plagioclase (Pl) and green diopsidic pyroxene (Di), Lower Barun Valley, eastern Nepal. **(c)** tremolitic amphibole (Am) bearing calc-silicate rock, Chyamtang, Upper Arun Valley, eastern Nepal. **(d)** Ca-garnet / Ca-Mg-pyroxene rich calc-silicate rock, Chyamtang, Upper Arun Valley, eastern Nepal. **(e)** grossular bearing garnetite boudin (Grt), Tashigaon, Arun Valley, eastern Nepal.

Fig. 3 – Simplified geological map of the central-eastern sector of the Himalayan belt (modified from GOSCOMBE *et alii*, 2006; DASGUPTA *et alii*, 2004; MOSCA *et alii*, 2012; MOSCA *et alii*, 2013) showing sample locations subdivided in the CFMAS-HC and NKCFMAS-HC groups, as discussed in the text. White dotted lines are the geotraverses investigated since 2004. The double-dashed grey line is the approximate political boundary between Nepal to the south, west, China (Tibet) to the north, India (Sikkim) to the east. Inset shows the location of the study area (white rectangle) in the framework of the Himalayan chain. MCT: Main Central Thrust; MFT: Main Frontal Thrust; MBT: Main Boundary Thrust; STDS: South Tibetan Detachment System; E: Everest; K: Kangchenjunga; M: Makalu.

Fig. 4 - Schematic cross-section across the eastern Himalaya (modified from GOSCOMBE *et alii*, 2006, and SEARLE *et alii*, 2008) highlighting the structural location and field occurrence of CFMAS-HC **(b,c)** and NKCFMAS-HC **(c,d)** calc-silicate rocks. The arrows in (b) and (c) indicate the calc-silicate boudins. Selected mineral isograds relevant for the predominant lithologies are also shown. Abbreviations and colours of the different calc-silicate groups as in Fig. 3.

Fig. 5 - Representative microstructures of CFMAS-HC calc-silicate rocks. **(a)** Type A: tremolite-bearing impure marble. Crossed Polarized Light (XPL). **(b,c)** Type B: garnet + amphibole + zoisite –bearing calc-silicate rock. The detail in (c) shows plagioclase replacing zoisite. Plane Polarized Light (PPL). **(d,e)** Type C: garnet + clinopyroxene calc-silicate rock. Garnet-rich layer, characterized by garnet + quartz intergrowths and by the presence of abundant graphite flakes (d: PPL; e: XPL). **(f,g)** Type D: clinopyroxene-bearing calc-silicate rock (f: PPL; g: XPL).

Fig. 6 - Representative microstructures of NKCFMAS-HC calc-silicate rocks. **(a,b)** Type A: muscovite + phlogopite impure marble (a: XPL; b: PPL). **(c,d)** Type B: muscovite + biotite + calcite –bearing phyllitic micaschist. Note the unusual greenish-brownish pleochroism of biotite and the presence of discontinuous calcite domains intercalated to the siliciclastic layers (c: PPL; d: XPL). **(e,f)** Type C: muscovite + biotite + scapolite + garnet micaschist (e: PPL; f: XPL). **(g,h)** Type D: biotite + scapolite –bearing calc-silicate gneiss (g: PPL; h: XPL). **(i.j)** Type E: K-feldspar + scapolite + epidote + amphibole + clinopyroxene calc-silicate gneiss. Note the coexistence of amphibole and clinopyroxene (i: PPL; j: XPL). **(k,l)** Type G: K-feldspar + scapolite + clinopyroxene + calcite calc-silicate granofels (k: PPL; l: XPL).
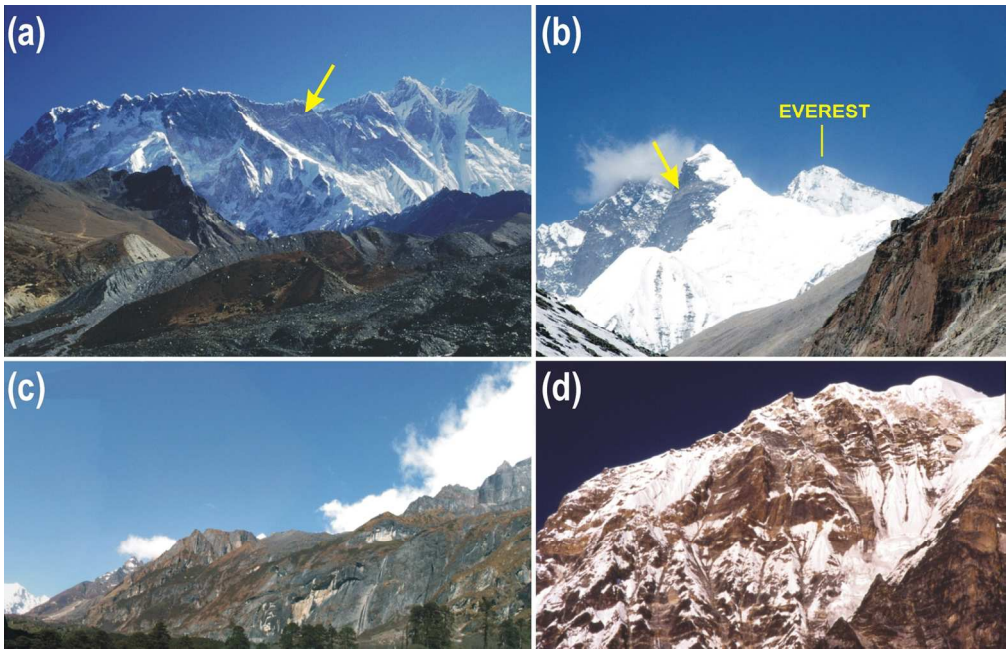
Fig. 7 – (a,b) Simplified isobaric T-X(CO_2) phase diagrams sections calculated for activity-corrected end-members, for CMFAS-HC (type C) calc-silicate rocks (a) and NKCFMAS-HC (type F) calc-silicate rocks (b) from the GHS-L and GHS-U, respectively. The composition of the solid solutions (a: garnet; b: scapolite and plagioclase) changes continuously along the isobaric univariant curves. Solid large points are isobaric invariant points; empty points are isobaric singular points (i.e. points at which the stoichiometric coefficient of one phase vanishes, such that this phase behaves

as a reactant on one side of the reaction and as a product on the other side of the reaction). The relevant isobaric univariant reactions (e.g. 24b) and invariant points (e.g. I26') are numbered and reported in the insets (the prefix I denotes the isobaric invariant points). Isobaric univariant curves labeled with the same number but with different suffix (e.g. 24a, 24b and 24c in (a)) are characterized by one or more singular points: this means that the different portions of these curves involve the same phases, but some of these phases behave alternatively as a reactant or as a product. Coloured points and curves refer to the reactions relevant to explain the microstructures observed in the studied calc-silicate rocks. The composition of the fluid circulating during the metamorphic evolution of the studied calc-silicate rocks is highlightened in the rectangular coloured boxes. **(c,d)** Simplified mixed-volatile P–T projections in the system CF(M)AS-HC (c) and NKC(F)MAS-HC (d), respectively, with a selection of the univariant curves "seen" by the studied samples (see GROPPO *et alii*, 2013 and GROPPO *et alii*, submitted for further details). Each univariant curve corresponds to an isobaric invariant point (see dotted arrows connecting the isobaric invariant points in (a) and (b) with the correspondent univariant curves in (c) and (d)). The relevant univariant reactions (e.g. U26c) are numbered and reported in the insets (the prefix U denotes the "truly" univariant reactions in the mixed volatile P-T projections). Univariant curves labeled with the same number but with different suffix (e.g. 26a, 26b. 26c and 26d in (c)) are characterized by one or more singular points: this means that the different portions of these curves involve the same phases, but some of these phases behave alternatively as a reactant or as a product. The compositions of the solid solutions (c: garnet; d: scapolite and plagioclase) and of the fluid phase (c and d) change continuously along the univariant curves. Solid small points indicate the variation of fluid (c,d), garnet (c), plagioclase and scapolite (d) compositions along each univariant curve; empty points are singular points. The variations of fluid (F: $X(CO_2)$), garnet (X_{Grs}), plagioclase (X_{An}) and scapolite (eqAn) compositions along each univariant curve are also reported. The P–T evolution inferred from the hosting anatectic paragneiss (c: GROPPO *et alii*, 2009; d: GROPPO *et alii*, 2012) is reported with grey arrows. Coloured points and curves refer to the reactions relevant to

explain the microstructures observed in the studied calc-silicate rocks. The composition of the fluid circulating during the metamorphic evolution of the studied calc-silicate rocks is highlightened in the rectangular coloured boxes.

139x89mm (300 x 300 DPI)

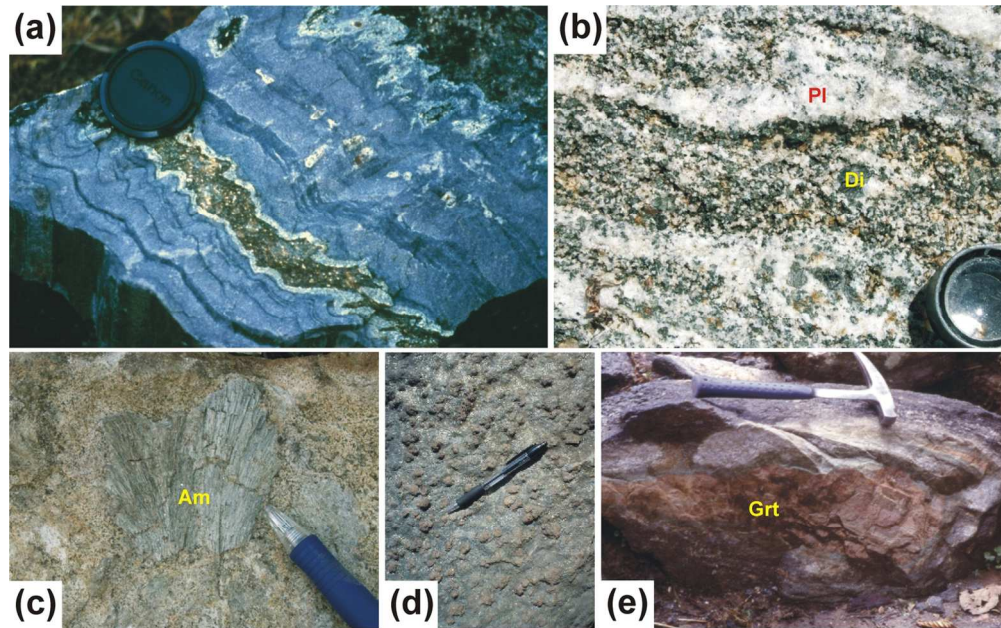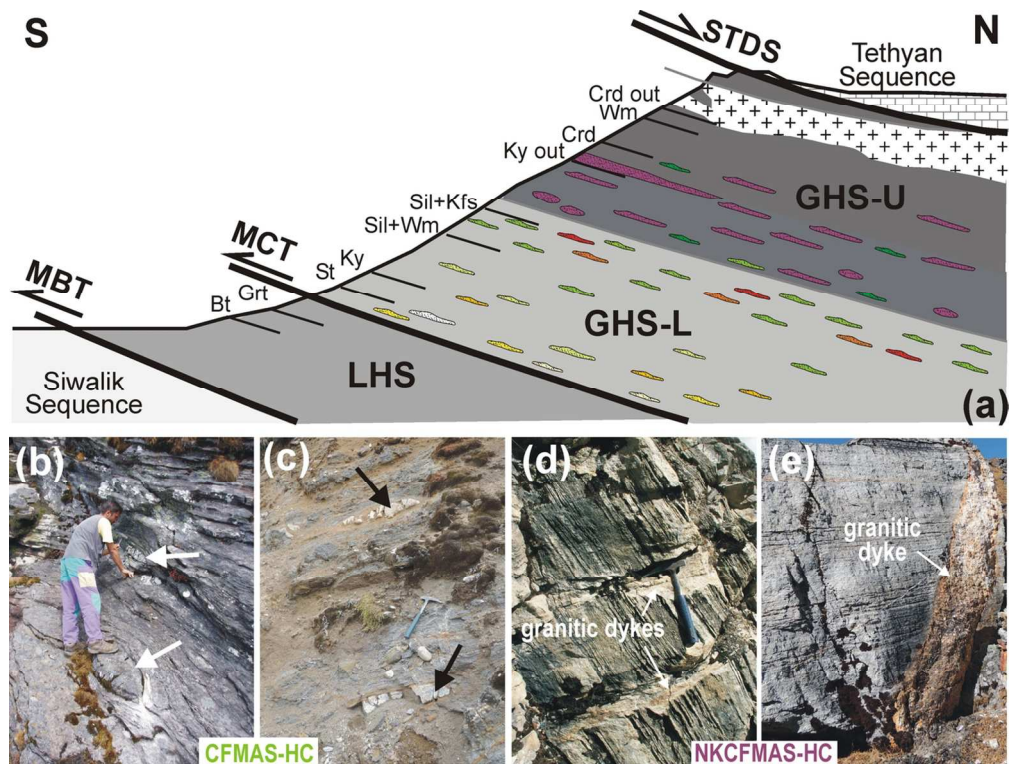131x81mm (300 x 300 DPI)

122x92mm (300 x 300 DPI)

167x126mm (300 x 300 DPI)

1
2
3
4
5
6
7
8
9
10
11
12
13
14
15
16
17
18
19
20
21
22
23
24
25
26
27
28
29
30
31
32
33
34
35
36
37
38
39
40
41
42
43
44
45
46
47
48
49
50
51
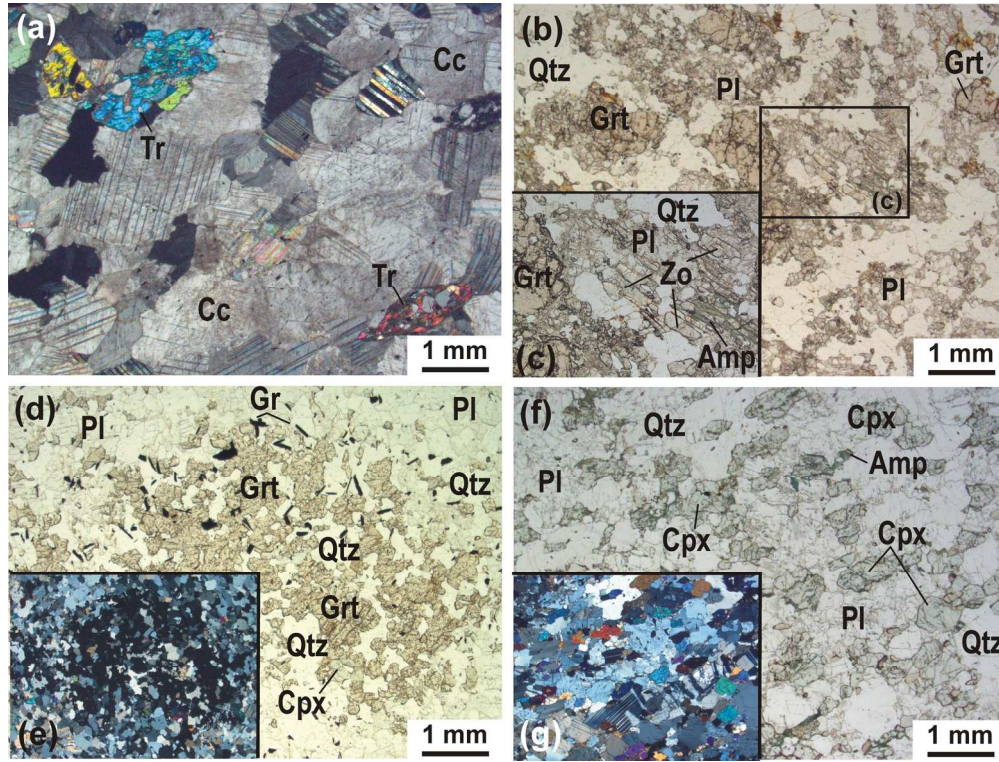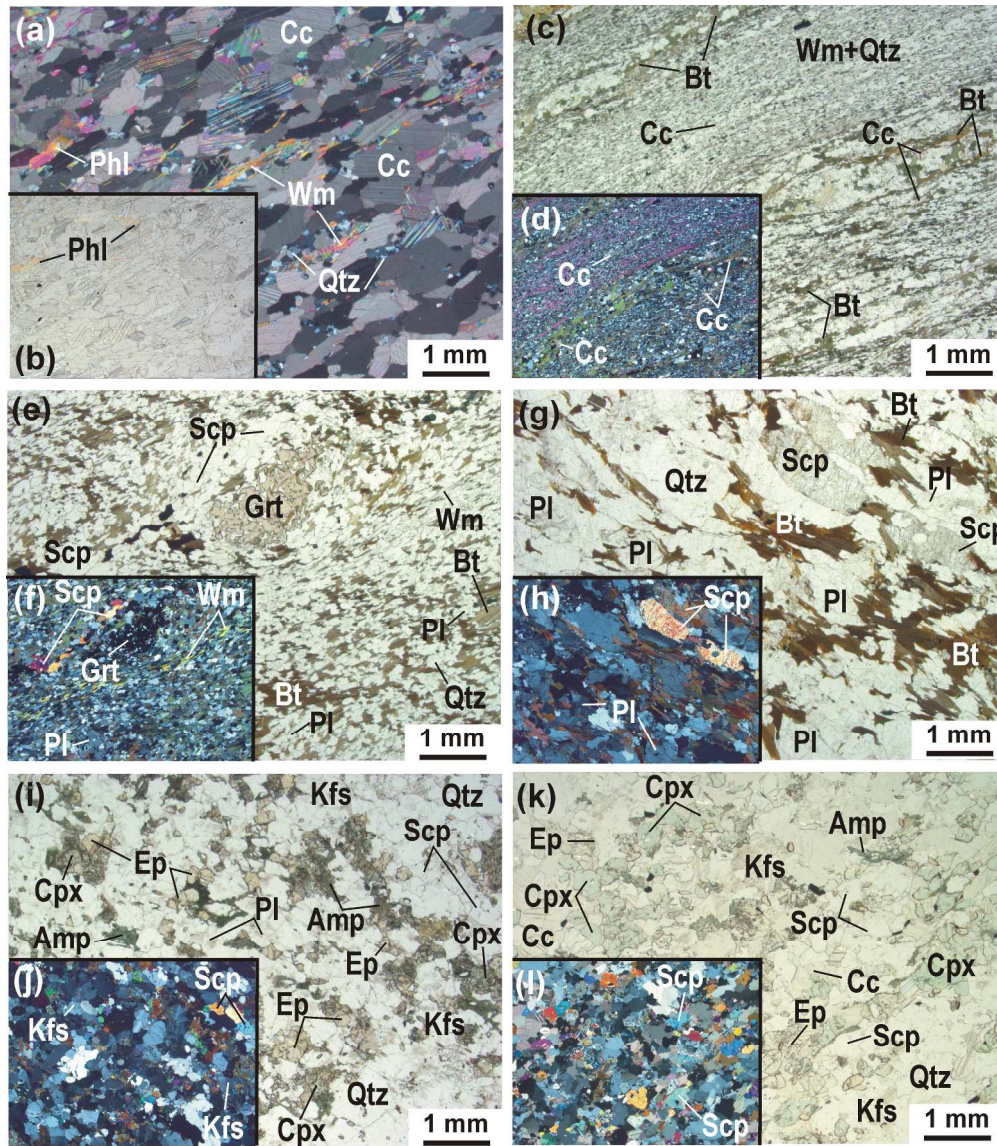52
53
54
55
56
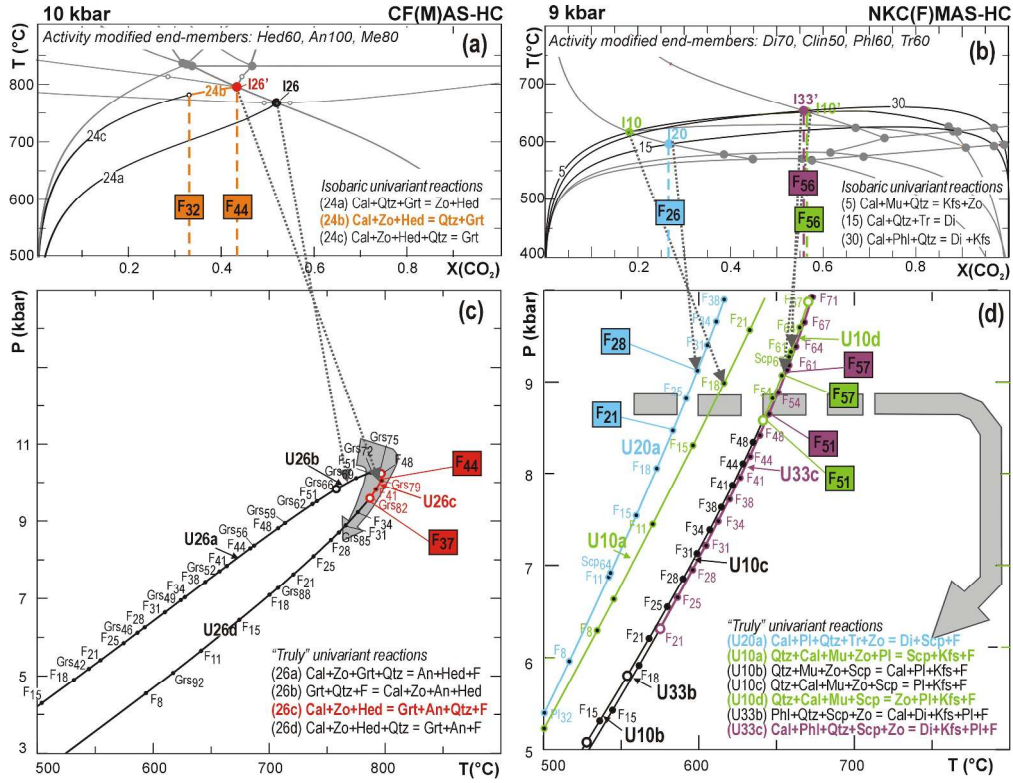57
58
59
60

253x289mm (300 x 300 DPI)

329x254mm (300 x 300 DPI)

Table 1 - Equilibrium assemblages and mineral abundances for each of the calc-silicate types

	Cal	Qtz	Pl	Zo/Ep	Scp	Wm	Bt	Kfs	Amp	Cpx	Grt	Gr	Ttn	Turm	Aln
CFMAS-HC calc-silicate group															
(A)	x x x x x	- / x	- / x						x x			x	x		
(B)		x x x	x / x x x	x / x x x					x / x x		x x x		x		
(C)		x x x	x / x x x	x / x x						x x / x x x	x x / x x x	x	x		
(D)		x x x	x x	- / x						x x x			x		
NKCFMAS-HC calc-silicate group															
	Cal	Qtz	Pl	Zo/Ep	Scp	Wm	Bt	Kfs	Amp	Cpx	Grt	Gr	Ttn	Turm	Aln
(A)	x x x x x	x x	- / x			x / x x	x / x x		- / x			- / x	x	x	
(B)	x / x x x	x x x	x / x x			x x / x x x	x x / x x x						x		
(C)		x x x	- / x x	- / x x	- / x x	x / x x	x x / x x x				x		x		
(D)		x x x	x / x x	- / x	x / x x		x x / x x x	- / x x					x		
(E)		x x / x x x	x / x x	- / x x	- / x		- / x x x	x / x x x	x x x	- / x			x		
(F)	- / x x	- / x	x / x x	- / x	x / x x x			x / x x x		x x / x x x			x	x	x

Mineral modes are qualitatively reported (- = not present; x = scarce; x x x x x = very abundant). Retrograde phases are not indicated.